Experimental Thermal and Fluid Science 62 (2015) 192–201

Contents lists available at ScienceDirect

Experimental Thermal and Fluid Science

journal homepage: www.elsevier.com/locate/etfs

Experimental and numerical analysis of free surface deformation in an electrically driven flow

A. Kharicha [a,*], I. Teplyakov [b], Yu. Ivochkin [b], M. Wu [c], A. Ludwig [c], A. Guseva [b]

[a] Christian Doppler Laboratory for Advanced Process Simulation of Solidification and Melting, University of Leoben, 8700 Leoben, Austria
[b] Joint Institute for High Temperatures of Russian Academy of Sciences, Moscow, Russia
[c] University of Leoben, 8700 Leoben, Austria

ARTICLE INFO

Article history:
Received 21 February 2014
Received in revised form 29 October 2014
Accepted 25 November 2014
Available online 10 December 2014

Keywords:
Ampere's force
Lorentz force
Magnetohydrodynamic
Free surface
Electric current
Liquid metal
Arc
Jet
Electric arc furnace
Pinch

ABSTRACT

The present paper presents the experimental and numerical results of an electrically induced flow in a cylindrical container (188 mm diameter) filled with a In–Ga–Sn alloy. The electric current is applied from copper electrodes of various diameters (4–8 mm) and varied from 100 to 700 A. The deformation of the free surface just under the electrode is reported in term of depth. At some critical current an arc develops around the electrode tip. To explore numerically what happens in such flows, calculations of the Magnetohydrodynamic (MHD) flow are performed. The numerical model is based on a potential formulation for the electromagnetic field. The evolution of the free surface flow is tracked with a VOF model. The electromagnetic parameters are fully coupled with the evolution of the free surface and the contact surface at the electrode. At low current density the interface is shifted downward by the pinch action of the Lorentz force. In the same time the rotational part of the Lorentz force drives the liquid metal flow in radial direction towards the electrode. The flow is accelerated towards the electrode and sinks in the form of a strong jet. At the high current density, the velocities are strong enough to induce further displacement of the interface by a Bernoulli mechanism. The combined action of the pinch and the rotational components of the Lorentz force on the interface displacement, scales as I^2. The numerical and experimental results are in good agreements.

1. Introduction

Electrically induced flows are present in many industrial processes such as Electroslag remelting, Vacuum arc remelting, electrolyzers, electric arc furnaces, smelting and aluminium reduction cells. The flow in such system is generated by the interaction of the electric current with the self-magnetic field. In these processes the interfaces between metal/electrolyte or electrode/Plasma are deformed by the electromagnetic force. Large difference in electric conductivity exists between the phases, metals are typically 10^3–10^5 times more conducting than the electrolyte and the plasmas. If an electric current density is exceeded a strong coupling could exist between the electric current distribution and the phase distribution. The study of the mechanism of generation and development of the flows generated within a current carrying fluid due to the interaction of an electric current with a self-magnetic field is important in order to gain correct understanding of these engineering processes. In spite of the practical significance, some essential features of these flows have not yet been explored.

One of oldest reference of an experiment showing the deformation of an interface was described by Northrup [15]. In one of his experiment he used a box of various cross section filled with a layer of liquid potassium–sodium. When a sufficiently strong horizontal current is applied, the level of liquid metal decreases vertically in the narrow section of the box. This phenomena is also known as Magnetohydrodynamic (MHD) "pinch effect", it is an instability in which the conductor constricts itself until severed. More recently Graneau [5] studied force generated by the application of a current in a propulsive seawater jet engine. To illustrate the mechanism, he considers an experiment in a cup filled with liquid mercury where a current was applied between an immersed copper rod and a copper ring. The rod was located in the bottom of the cup, and the ring just underneath the surface. A jet was generated and caused the surface to rise in the middle of the cup giving the aspect of a liquid mercury fountain. It was also shown that the jet propulsive force is proportional to the square of the current.

Simulation with interface movement under the action of electric current are mainly found in the field of aluminium reduction

* Corresponding author.
E-mail address: abdellah.Kharicha@unileoben.ac.at (A. Kharicha).

http://dx.doi.org/10.1016/j.expthermflusci.2014.11.014
0894-1777/

cells [2,3,14,22] and Electroslag remelting process [6,7,10]. Several mathematical models have been developed to simulate the hydrodynamics and the interface deformation. The most popular model is based on the "shallow layer" theory, motivated by the fact that the depth of the liquid layers are much smaller than the horizontal dimensions of the process. Full simulations in 3D are still challenging in term of numeric and calculation time [8].

The experimental investigation of flows in industrial processes is hindered by the fact that, due to high temperatures and chemical aggressiveness of the slag/cryolite, accurate direct measurement of the velocity are very difficult.

Attempts have been made to validate the numerical model used in the present work, with data collected in literature [9]. The validation aimed to numerically reproduce the intriguing experimental observations made by Bojarevics [1] on the appearance of swirl in flows in an electrically induced flow. The experiment consisted in supplying an electric current to a small water-cooled electrode of 0.8 cm diameters, in the centre of a free surface mercury filling a hemispherical copper container, 36 cm in diameter, which represents the other electrode. The electrode is electrically insulated in most of its length except over a short distance below the free surface. When the electric current is applied from above the free surface, a converging flow is set up. The flow is coupled with a rotation. No rotation is observed when the current is supplied from below the free surface. The prediction of the main features such as the deformation of the free interface as well as the swirl generation was in agreement with the experimental observation. The main conclusion was that the earth magnetic field had indeed a strong influence on the flow. Any analysis of an electrically induced flow should carefully account for the influence of external magnetic fields even as small as the one generated by the earth [21].

For the sake of further validation, new experiments and simulations were performed. The present paper presents an investigation of an electrically induced flow generated within a cylindrical container. In opposite to the Bojarevics [1] experiment, the electrode has spherical tip. Before the experiment the tip is fully immerged in the liquid metal, once a current is applied the interface starts to deform. To understand the physical mechanisms involved in these experiments, selected simulations were performed with a 2D MHD–VOF numerical model.

2. Experimental procedure

The experiment consists in filling a hemispherical container with the galistan alloy. A spherically tipped electrode is dipped within the liquid metal so that the entire tip is entirely in contact with the liquid metal. The experimental procedure and the dimensions of the facilities are given in Figs. 1 and 2. The current is applied from the top, and leaves from the bottom by traveling over a vertical wire strictly aligned with the electrode. The deformation of the interface is observed and measured optically with an optical camera. To obtain a good visibility of the electrode tip an angle of view of about 26° is set between the horizontal plane and the axis of the camera (Fig. 1).

3. Numerical method

In the present work only the 4 mm diameter electrode is numerically investigated. We assume the system being laminar and 2D axisymmetric. The equations for electric potential, magnetic potential vectors, as well as the velocity field are solved in a fully coupled and transient way. The coupling between the flow and the electromagnetic field is done through the possible movement of the metal/air interface which can modify the electric current path.

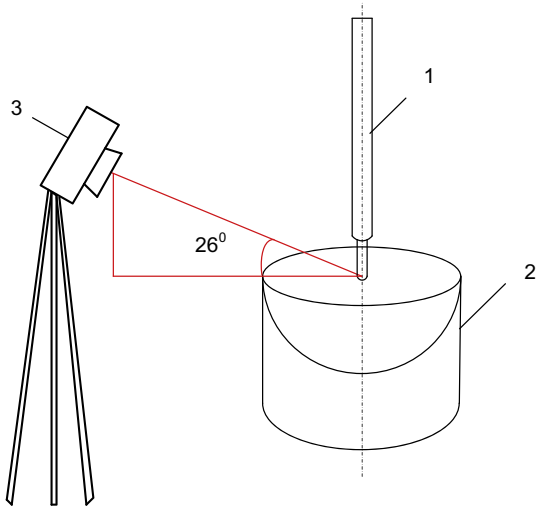

Fig. 1. Scheme of experiment. 1 – Electrode, 2 – container, 3 –photocamera.

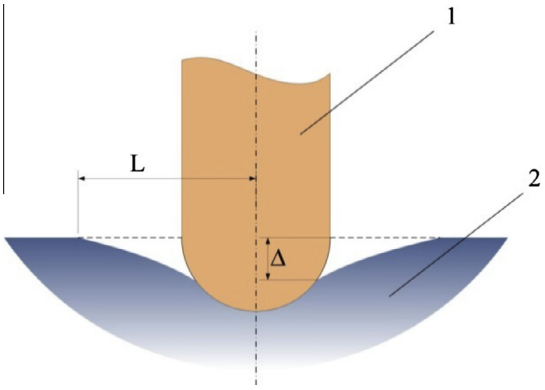

Fig. 2. Scheme of surface deformation Δ – depth of cavern, L – width of cavern, 1 – electrode, 2 – liquid metal In–Ga–Sn.

Table 1
Process parameters and averaged material properties used in the simulations.

In–Ga–Sn	
Density	6325 kg/m^3
Viscosity	0.0024 kg/m/s
Effective electric conductivity	1.0×10^6 $(\Omega\,m)^{-1}$
Interface tension with air	0.6 N/m
Copper	
Electric conductivity	4.5×10^7 $(\Omega\,m)^{-1}$
Air	
Density	1.1 kg/m^3
Viscosity	0.00017 kg/m/s
Electric conductivity	1.0×10^{-10} $(\Omega\,m)^{-1}$

The fluid calculation domain is a hemisphere divided into 100 000 volume elements. The mesh is refined at vicinity of all wall boundaries, especially near the electrode so that the area of interest is correctly resolved. The electrode radius is 4 mm. The properties of the materials are constant (Table 1). Except the electric conductivity, the values used are an average of the values reported in literature by Prohorenko et al. [17], Morley et al. [13], and Plevachuk [16]. Larger differences in the values exist between the measured electrical conductivity. The main reason is that the electrical conductivity is highly dependant on the exact proportion of the

alloy elements used in the Gallistan. In addition, when exposed to air, the alloy slowly oxidizes to form a Ga_2O_3 oxide layer. If mixed with the liquid metal the presence of oxide particles will decrease the effective electric conductivity. There exists also a dependance of the conductivity on temperature, however during our experiments the liquid metal temperature has generally not the time to reach very high values. Depending on the electrode diameter and electric current intensity, at the end of an experiment the temperature does not usually exceed 40–50 °C. Therefore the properties are assumed to be constant. In the present numerical investigation an effective value of the electrical conductivity of $10^6\ (\Omega\,\mathrm{m})^{-1}$ was chosen.

The electromagnetic domain includes the fluid domain and the electrode as well as the copper container (Fig. 3).

The interface between the two phases is tracked with a geometric reconstruction VOF technique. A single set of momentum equations is shared by the fluids, and the volume fraction of each of the fluids in each computational cell is tracked throughout the domain. According to the local value of the volume fraction f, appropriate properties and variables are assigned to each control volume within the domain. In a two phase system the properties appearing in the momentum equation are determined by the presence of the component phase in each control volume. The local values of a physical property Θ (such as density ρ, viscosity μ, electric conductivity σ) are interpolated by the following formula $\Theta = \Theta_1 f_1 + \Theta_2 f_2$, where the subscripts 1,2 indicate the corresponding phase, 1 for air, 2 for the alloy. All available and used properties are reported in Table 1. However the contact angle with copper is missing. From experimental observation (see Fig. 2), the contact angle can be estimated to be between 90° and 120°.

The third order resolution MUSCL scheme is used for the space discretisation of all conservation equations. The second order Crank–Nicolson method is used for the discretisation in time resolution. The time step is controlled through a chosen courant number of 0.1. The typical calculation time step lies in the range of 10^{-5}–10^{-3} s.

3.1. Electromagnetics

Let the typical root–mean–square velocity be u, L the typical length scale of the flow, and the magnetic diffusivity be $1/\sigma\mu_0$ where σ is the electrical conductivity and μ_0 is the magnetic permeability. All materials are assumed to be nonmagnetic, with a magnetic permeability equal to the vacuum magnetic permeability. The dimensionless parameter $Rm = uL\sigma\mu_0$ is known as the magnetic Reynolds number. We suppose that $Rm \ll 1$. If the magnetic Reynolds number is small (in other words the magnetic diffusion time is much smaller than other time scales), the fluctuations b of the magnetic field $\vec{B}+\vec{b}$ due to fluid motion are much smaller than the self-magnetic field $\vec{B}$ generated by the applied current I_0.

The electromagnetic field is solved by using the electric field ϕ and the magnetic potential vector $\vec{A}$. The electric potential equation is extracted from the equation of the conservation of the electric current:

$$\nabla\cdot\vec{j}=0 \text{ with } \vec{j}=-\sigma\frac{\partial\vec{A}}{\partial t}-\sigma\nabla\phi \tag{1}$$

The total current $\vec{j}$ is the sum of the imposed current $-\sigma\nabla\phi$ and the eddy current $-\sigma\frac{\partial\vec{A}}{\partial t}$ generated by the time variation of the magnetic field. Outside the liquid and the electrode domain no electric current is assumed to exist. A constant and uniform electric current flow is applied at the bottom boundary of the container domain, and a constant electric potential ($\phi = 0$) is applied at the top of the solid electrode.

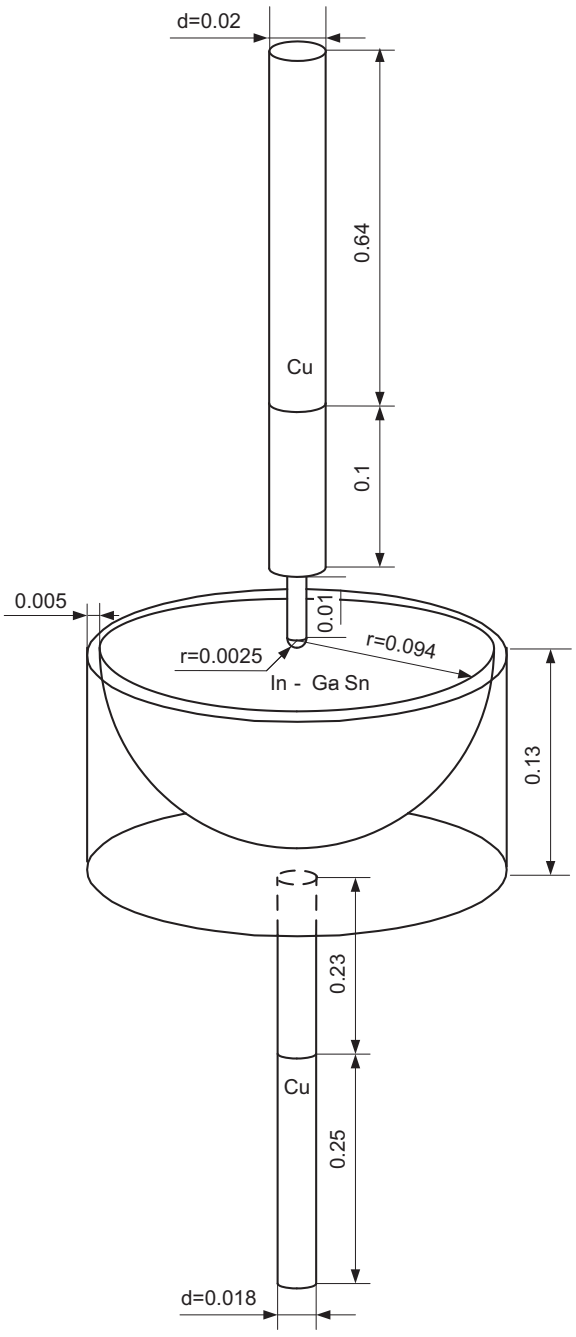

Fig. 3. Dimension of the facility. The electrode represented in the scheme is the 0.005 m diameter electrode. Unit of dimension is meter.

The magnetic field $\vec{B}$ is extracted by solving the magnetic potential vector $\vec{A}$ equation.

$$\nabla\times\left(\frac{1}{\mu_0}\nabla\times\vec{A}\right)-\nabla\left(\frac{\lambda}{\mu_0}\nabla\cdot\vec{A}\right)=\vec{j}, \tag{2}$$

with:

$$\vec{B}=\vec{\nabla}\times\vec{A} \tag{3}$$

The uniqueness of the magnetic potential vector is ensured by the fact that Eq. (2) uses the Coulomb gauging. A penalty function term $-\nabla\left(\frac{\lambda}{\mu_0}\nabla\cdot\vec{A}\right)$ is used in order to enforce the zero divergence of the

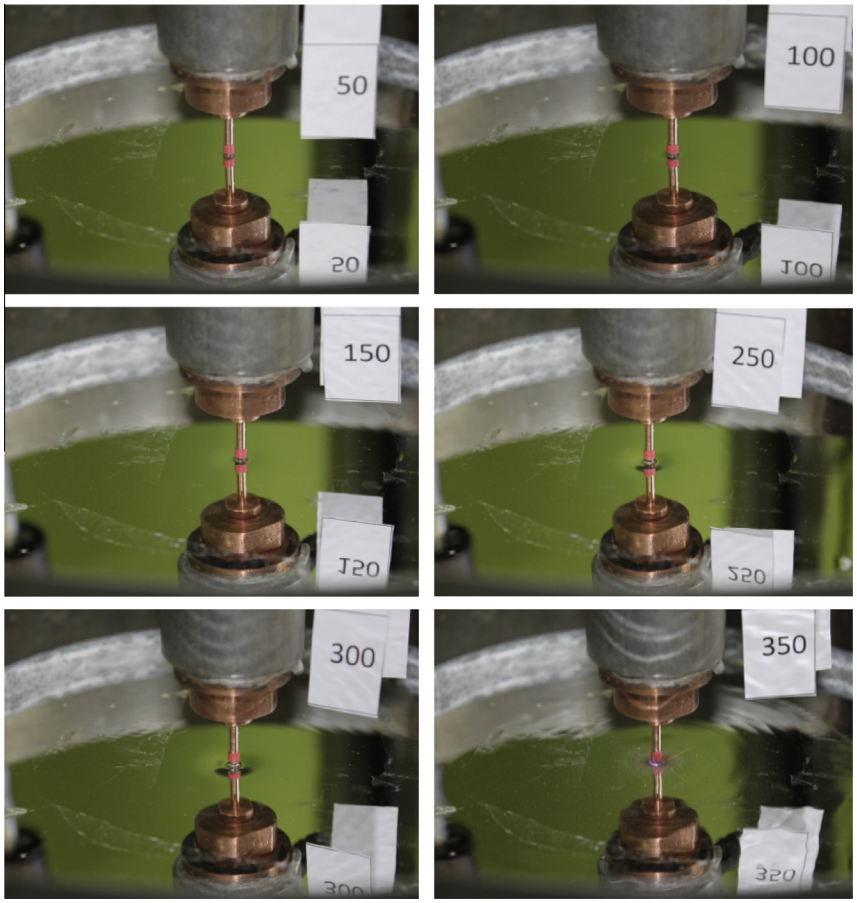

Fig. 4. Surface of the liquid metal for the case of 5 mm electrode diameter. A plastic gain of pink colour surrounds the tip of the electrode. The applied DC current is 50, 100, 150, 250, 300 and 350 A. Circular waves are visible for $I > 250$ A. A dark area near the electrode appear when the cavern becomes deep and wide enough. For $I = 350$ A an arc appears around the electrode tip. (For interpretation of the references to colour in this figure legend, the reader is referred to the web version of this article.)

magnetic field, in which the penalty factor λ is chosen to be equal to 1.

In the liquid the computed electromagnetic field is dynamically adjusted from the space distribution of the electric conductivity, which is in turn a function of the predicted phase distribution. Once the electric and magnetic field solved, the time and space dependant Lorentz force acting on liquid alloy is defined by:

$$\vec{F}_L = \vec{j} \times \left(\vec{B} + \vec{B}_{earth} \right) \tag{4}$$

where $\vec{B}_{earth}$ is the vertical component of the earth magnetic field, which is downward oriented in the Nordic hemisphere. The electric current and the induced magnetic field are fully coupled with the phase distribution. The influence of the axial component of the earth magnetic field is added to the magnetic field induced by the electric current.

3.2. Fluid flow

The motion of the metal and the air $\vec{U}$ is computed with the Navier–Stokes equations. In the present model the flow is assumed laminar. The non-slip condition is applied at all walls. The Lorentz force (Eq. (4)) is applied as a source term in the momentum equation:

$$\frac{D\rho\vec{U}}{Dt} = -\nabla p + \nabla\left(\mu\nabla\vec{U}\right) + \vec{F}_L, \tag{5}$$

where p is the static pressure.

4. Experimental results

A typical experiment is shown in Fig. 4. An insulating gain of pink colour surrounds the tip of the electrode, this element is used as a marker, the lower edge of tube is zero point. Notice the image reflexion produced by the clean metallic surface.

In order to obtain a better accuracy for very small displacement (<0.3 mm) the distance between edge of tube and its reflection on the deformed surface of liquid metal (on photo) is measured. For small displacement of the liquid metal, the surface inclination can be neglected, so that the measured distance is then simply divided by 2. For larger displacements the size of the emerged part of the electrode tip starts to be different from its reflexion on the metallic surface. In this case the reflected image is not taken into account in the measurement. Based on a comparison of the pixel size with the electrode diameter, the accuracy of the measurement is estimated to be better than 0.02 mm. Qualitatively the magnitude of surface deformation can be estimated by the extend of the dark region just under the electrode tip (Fig. 4). Circular waves are clearly seen on the liquid metal surface for applied current exceeding 250 A. When the applied current exceeds a critical current an arc surrounding the electrode tip appears (Fig. 4). Except for the 5 mm electrode diameter, the critical current for the arc appearance increases with the electrode diameter. Visually the surface roughness of the 5 mm electrode was found to be higher than that of the other electrodes. The state of the electrode surface can probably explain the discrepancy in term of arc appearance for this electrode.

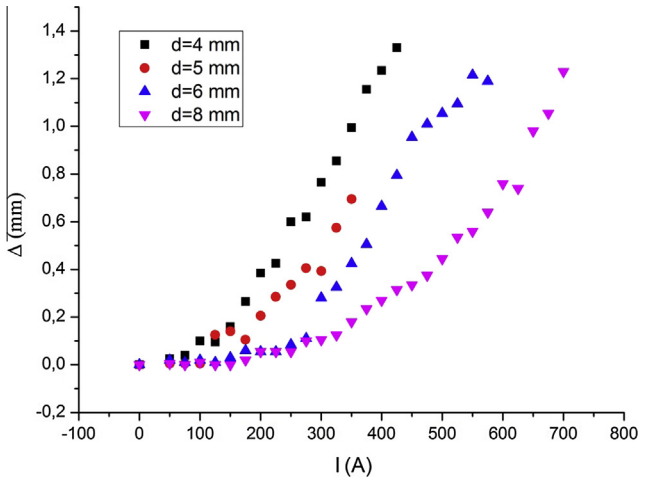

Fig. 5. Apparent cavern depths observed experimentally for different electrode diameter versus the applied current. The electric current for each electrode diameter is limited by the appearance of the arc.

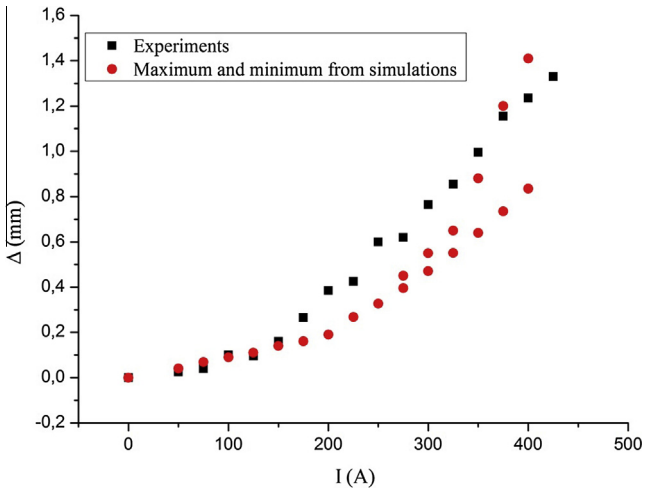

Fig. 7. Predicted against experimentally observed cavern depths for the case of 4 mm electrode diameter. In the simulations the position of the interface is unstable for $I > 275$ A.

Different experiences were performed with different electrode diameters (4–8 mm). The cavern depth increases with the applied current (Fig. 5). The measurements were no more possible as soon as the arc appeared. The increase is faster for small electrode than larger ones and the depth seems to vary quadratically with the applied current.

5. Numerical results and discussion

The numerical analysis focuses on the case of the 4 mm diameter electrode. Since the contact angle α is not known, simulations were performed with $I_0 = 350$ A for $\alpha = 120°$ and 90°. The deformation of the interface is very clear in figures (Fig. 6). The case of $\alpha = 120°$ gives the deepest cavern (Fig. 6) and the best fit with the experimental data (Fig. 7), this case will be presented and discussed in detail.

The electric current density (Fig. 8) is very high within the electrode (10^7 A/m^2) with a maximum at the level of the liquid metal interface (3.8×10^7 A/m^2). Within the liquid the maximum magnitude is smaller (10^7 A/m^2), electric current density decreases with the inverse of the square of the radius. The system being

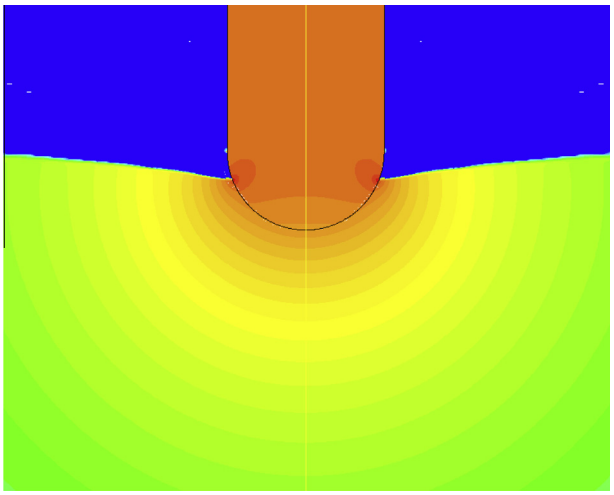

Fig. 8. Electric current density for $I = 350$ A, $d = 4$ mm, $\alpha = 120°$. (0 (blue) – 3.5×10^7 A/m^2 (red)). (For interpretation of the references to colour in this figure legend, the reader is referred to the web version of this article.)

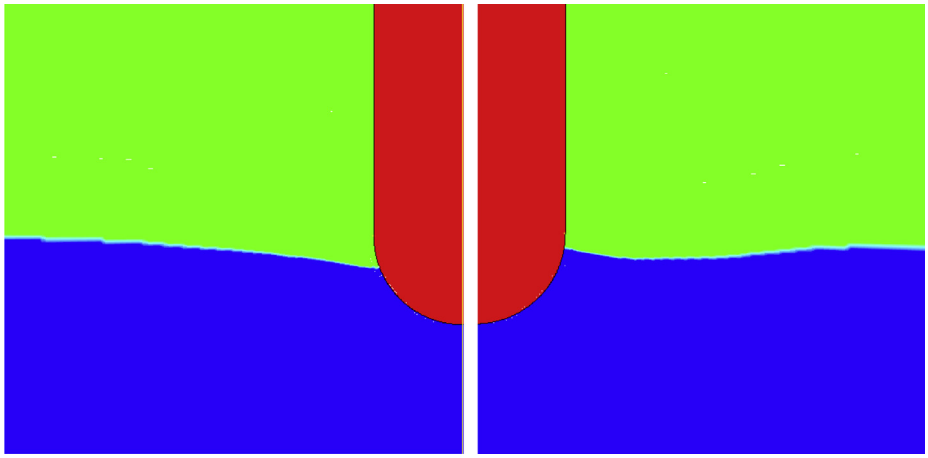

Fig. 6. Deformation of the interface predicted from simulations for electrode diameter 4 mm and for $I = 350$ A. (Red: electrode, Green air, blue: liquid metal). (For interpretation of the references to colour in this figure legend, the reader is referred to the web version of this article.)

axisymmetric, the self-magnetic field (Fig. 9) is aligned in the tangential direction ($B = B_\theta$), the maximum is reached on the surface of the electrode (0.035 T). In Fig. 10 the resulting Lorentz vector field shows circular (actually spherical) patterns. The very high magnitude Lorentz force (10^5–10^6 N/m^3) just under the electrode drives the flow in the form of a strong jet along the axis of symmetry (Fig. 11). The circulation of flow is closed through a large loop that fills the entire cavity. At the free surface close to the wall an additional smaller circulation is predicted.

The interaction of the earth magnetic field (Bz = −0.0005 T) with the current generates a Lorentz force in the tangential direction. Its magnitude (Fig. 12) is much smaller than the meridional one. The prediction shows that the swirling mainly occurs within the descending jet (Fig. 13). On the surface of the jet about 2 mm from the axis, the swirl velocity (0.12 m/s) represents 50% of the axial velocity (0.25 m/s), which means that the jet can be considered as swirling. Within the entire jet volume the swirl kinetic energy represents 15% of the total kinetic energy. But on the scale of the hemisphere, the angular kinetic energy represents only 5% of the poloidal flow kinetic energy.

Experimental analysis of bifurcation and transition in pressure driven round jets have been extensively studied in the past. However it is not clear if these results can be applied to an electrically driven and weakly swirling jet. Experiments on scalar-mixing behaviour in non-reacting jets indicate a qualitative transition in the turbulence and turbulent-mixing behaviour for Reynolds numbers in the vicinity of 10^4 [4]. Liepmann and Gharib [11]. In the case of the present round, turbulent jets, the characteristic velocity can be taken as the local centreline velocity of the jet ($U \sim 0.5$ ms), while the local length scale is typically taken as the local jet diameter (5 mm). The resulting Reynolds number is 7000, which is below but close to the critical number Reynolds reported for the transition to turbulence. However at such high Reynolds number one cannot exclude the possibility to have the generation of turbulence by intermittency. According to literature survey, the round jet is surely unstable and chaotic [19,18,12]. However the results of present simulation show limited level of instabilities, even for 400 A fluctuations represent less than 3% of the average values. These flow velocity fluctuations are generated by the unsteady movement of the interface near the electrode. Although the very small mesh size, 1e−5 m near the walls and within the jet, and 1e−3 m in the bulk, the predicted eddies are quite large. In addition the use of a 2D axisymmetric hypothesis strongly limits the number of possible non-linear interactions in the present numerical model.

The resulting shape is determined by the balance between buoyancy, the surface tension, and the Lorenz forces. Due to the obtuse contact angle, the surface tension is oriented in the down-

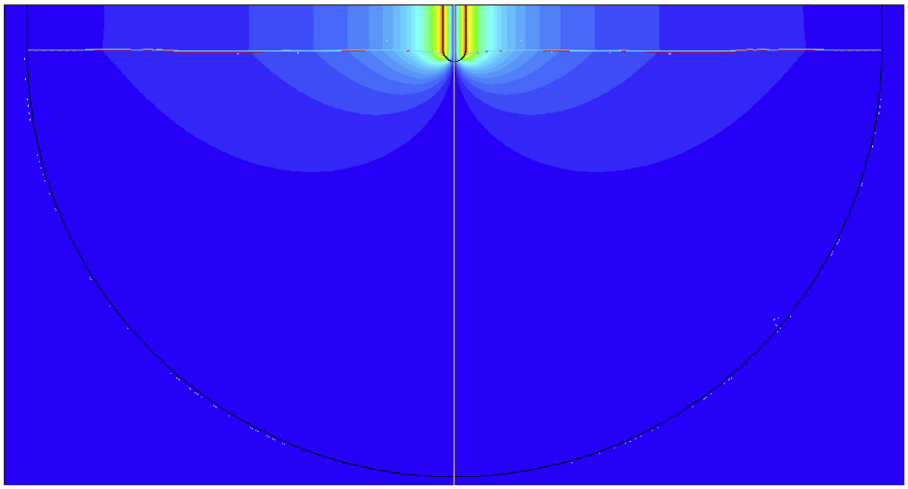

(a) Global distribution

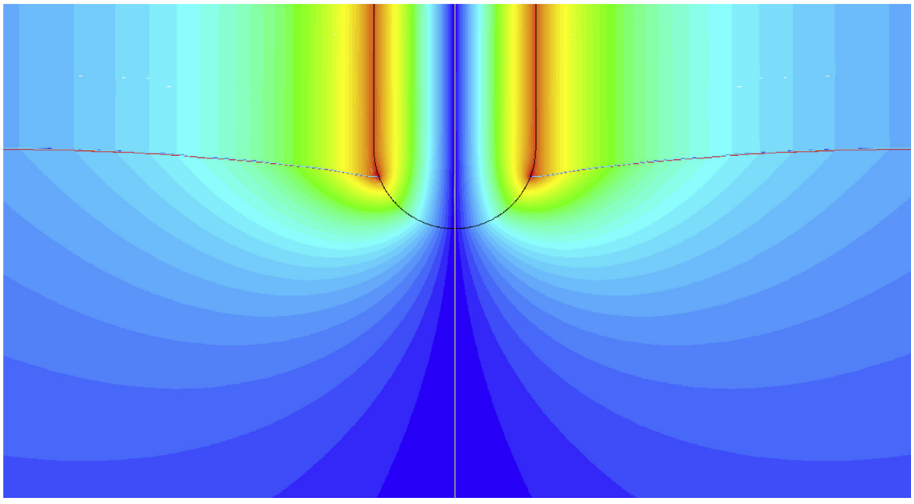

(b) zoom at the electrode tip

Fig. 9. Magnitude of the self-magnetic field for $I = 350$ A, $d = 4$ mm, $\alpha = 120°$. (0 T (blue) – 0.035 T (red)). (For interpretation of the references to colour in this figure legend, the reader is referred to the web version of this article.)

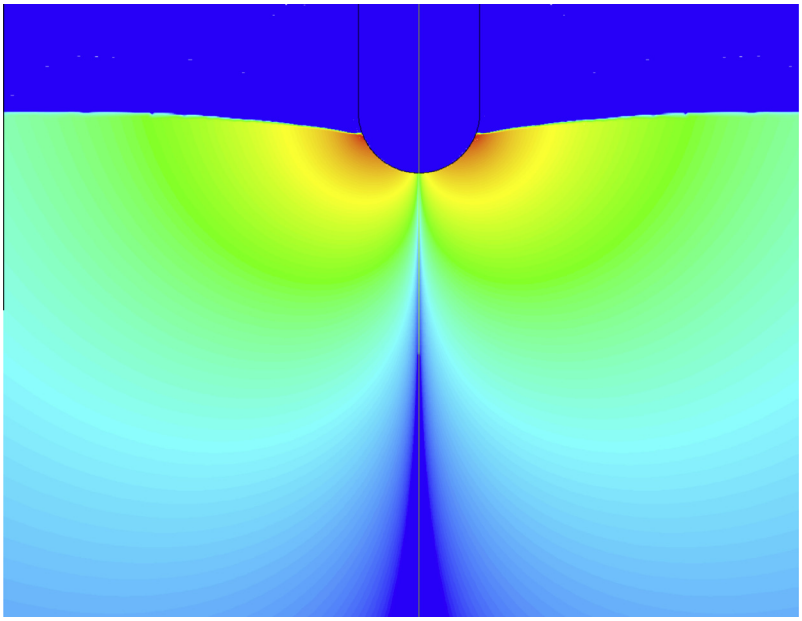

Fig. 10. Distribution of the meridional component of the Lorentz force for $I = 350$ A, $d = 4$ mm, $\alpha = 120°$. (0 (blue) – 10^6 N (red)). (For interpretation of the references to colour in this figure legend, the reader is referred to the web version of this article.)

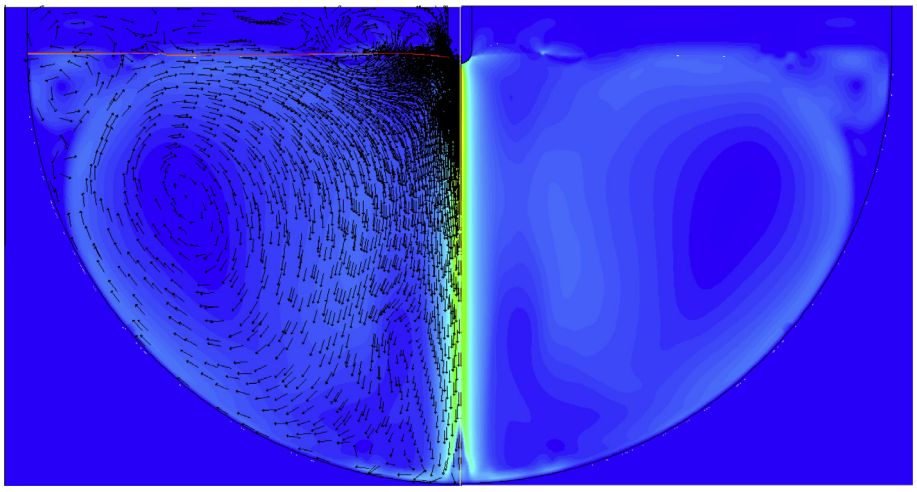

Fig. 11. Meridional velocity field $I = 350$ A, $d = 4$ mm, $\alpha = 120°$. (0 (blue) – 0.7 m/s (red)). (For interpretation of the references to colour in this figure legend, the reader is referred to the web version of this article.)

ward direction. Any further displacement of the interface must only be the result of the action of the electromagnetic forces. The Lorentz forces which increase with square of the current, have two different contributions. The first is the electromagnetic pinch force which acts perpendicularly to the liquid metal surfaces. The second effect is related to acceleration the flow towards the electrode, decreasing the static pressure due to a Bernoulli effect in the liquid metal. This hydrodynamic effect is due to the rotational part of the Lorentz force, it is usually neglected as in the early analysis made by Northrup [15]. If we assume an equilibrium between buoyancy and the Lorentz force:

$$\Delta \sim \alpha \frac{I^2}{\rho g}, \tag{5}$$

this is the main trend observed in Figs. 5 and 7. The factor alpha adds both the pinch and rotational effects of the Lorentz forces. A change in the increase rate is visible at around 100–200 A. This change in slope can be explained by the fact that for low applied current the pinch effect dominates, while at higher current the decrease of pressure due to the flow acceleration dominates. Taking an example based on Fig. 11, just before sinking under the electrode the liquid metal velocity reaches a speed of about $U \sim 0.1$ m/s, with a crude estimation this velocity can potentially induce a depression of about $U^2/2\,g \sim 0.5$ mm.

The shape of the electrode tip can easily lead to unstable configurations. As the electric current intensity is increased, the effective electrode radius (at the level of the interface) becomes smaller and smaller. Similarly the inclination of the electrode surface becomes less vertical and more horizontal. Due to the 120° contact angle the liquid metal inclines until the surface reaches an equilibrium becomes difficult especially for the surface tension force which tries to keep the required contact angle. If the Lorentz force is not quickly balanced, either by buoyancy or by surface tension, the contact area will fluctuate.

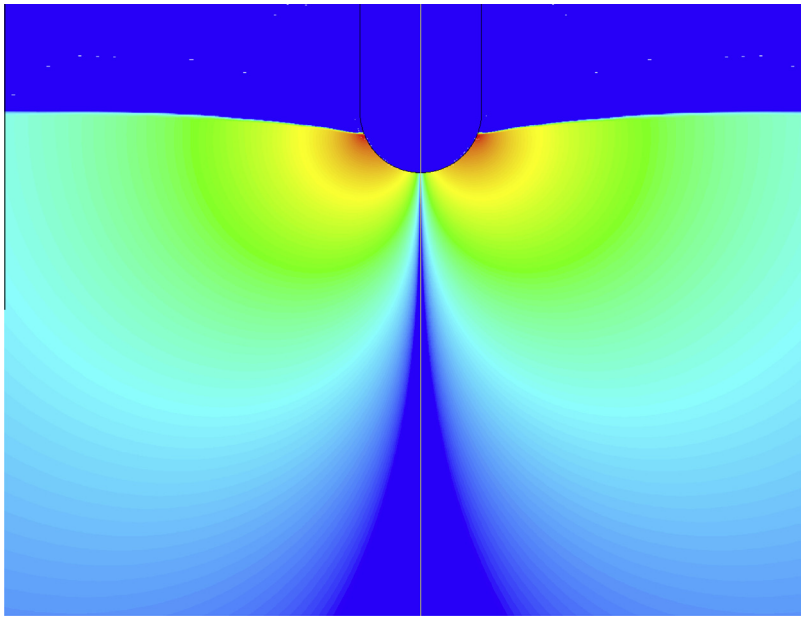

Fig. 12. Tangential component of the Lorentz force $I = 350$ A, $d = 4$ mm, $\alpha = 120°$ (0 (blue) – 1400 N (red)). (For interpretation of the references to colour in this figure legend, the reader is referred to the web version of this article.)

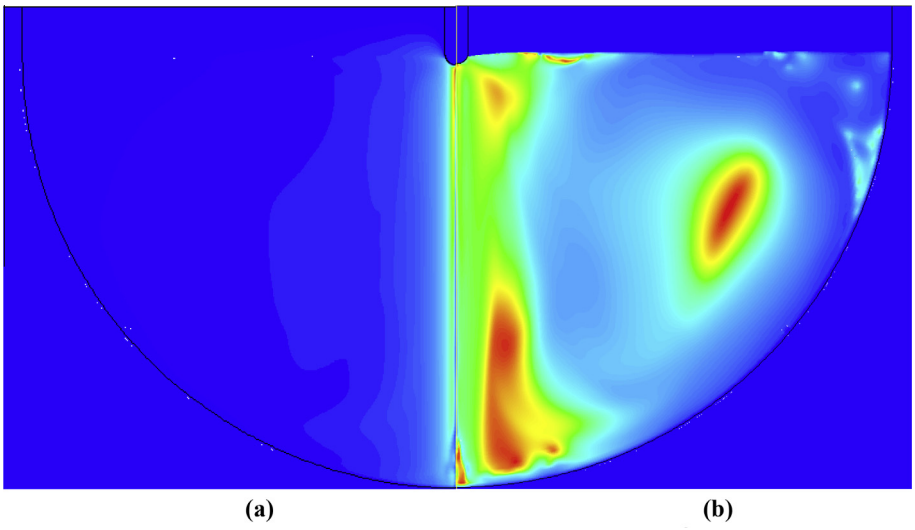

Fig. 13. (a) Swirl velocity magnitude $I = 350$ A, $\delta = 4$ mm, $\alpha = 120°$ (0 (blue) – 1400 N (red)), (b) ratio swirl velocity over the velocity magnitude (1 (red), 0 (blue)). (For interpretation of the references to colour in this figure legend, the reader is referred to the web version of this article.)

Instability at higher electric current density is attributed to the well-known coupling mechanism between electromagnetic pinch and the surface tension. The importance of this instability depends on the orientation of the liquid metal interface. When the interface is inclined as in Fig. 6 (120°), the radial component of the pinch force is positive, i.e. oriented in the outward direction (see Fig. 14a). The inclination of the liquid metal surface at the electrode can be determined with axial the position of the interface (Δ) and the contact angle α. At a critical Δ_C the interface becomes perfectly horizontal (Fig. 14b). This point is reached at:

$$\Delta_c = \frac{d}{2}\cos(\pi - \alpha). \tag{6}$$

In our case $\Delta_c = 1$ mm. If $\Delta > \Delta_c$ the contact angle will force the slope of the interface to be in the downward direction (Fig. 14c). Surface tension force is now oriented upward in the vertical direction, but the inward radial direction. The electromagnetic pinch force will act perpendicularly to the surface, i.e. in the radial down and inward directions. If the current density is high enough the combined surface tension and buoyancy would not be able to compete with the electromagnetic force. Since the contact line must follow the surface of the electrode, a slight descend of the liquid metal surface corresponds to a large shift in the radial direction. By an amplification mechanism, the contact area of liquid metal with the electrode can suddenly squeeze until contact is lost. This mechanism could explain the appearance of arc when the cavern exceed sufficiently the threshold Δ_c.

However experimentally no contact lost was observed prior to the appearance of the arc. An arcing will take place immediately if the contact is lost, but side arcing can also exists while the liquid metal is still in contact with the electrode. This scenario is highly supported by the very early appearance of the arc for the case of

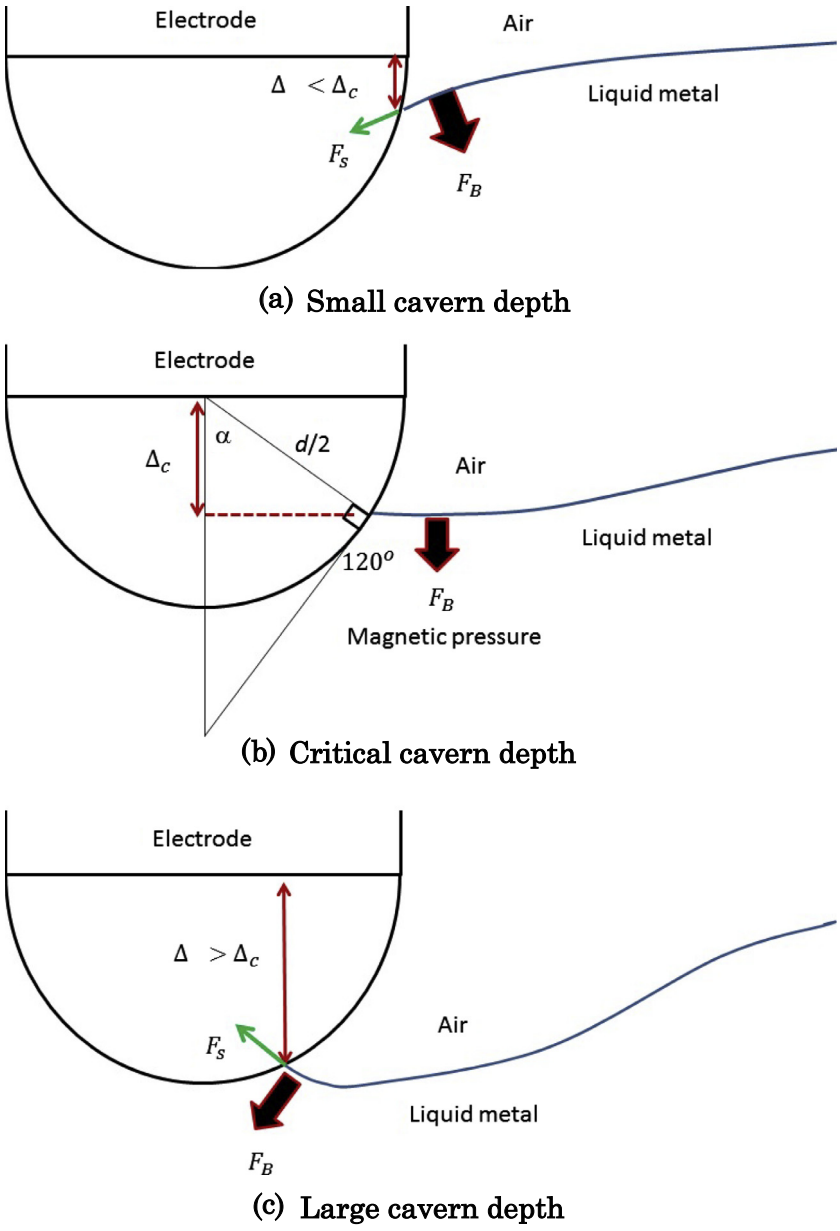

Fig. 14. Critical depth Δ_C defined as the depth at which the liquid/air interface becomes horizontal. F_B and F_S represent the direction of the magnetic pressure and the surface tension forces at the electrode-metal-air.

5 mm electrode (Fig. 5). The geometry and the surface conditions of the electrode and the liquid metal are probably important factors controlling the electric breakdown. Further investigations are necessary in order to distinguish between these two scenarios.

The adhering and wetting properties of the galistan alloy is not well. The role of surface tension is likely to be important especially during the displacement of the interface. While the numerical model has used a single wall contact angle, experimentally many liquids shows different contact angle depending on the direction of movement [20]. Depending on whether the electrode is dipped into or taken out of the galistan alloy, the authors have noticed a change in wetting properties.

6. Conclusions

The deformation of a free surface by the application of an electric current has been experimentally and numerically studied. The liquid In–Ga–Sn alloy was contained within a cylindrical container filled. The electric current was applied from copper electrodes of various diameters and varied from I = 100–700 A. At low current density the interface is shifted downward by the pinch action of the Lorentz force. In the same time the rotational part of the Lorentz force drives the liquid metal flow in radial direction towards the electrode. The flow is accelerated towards the electrode and sinks in the form of a strong jet. At the high current density, the velocities are strong enough to induce further displacement of the interface by a Bernoulli mechanism. The combined action of the pinch and the rotational components of the Lorentz force on the interface displacement, scales as I^2. The numerical and experimental results are in good agreements.

Experimentally an arc develops around the electrode when the applied current exceeds a critical value. Just before the arc develops the electrode was still in good contact with the liquid metal. At the present stage it is not yet clear on whether the arc develops

because of contact lost or because of the occurrence of an electric gas breakdown near the electrode surface. In the later mechanism, the electric current would flow in parallel in the liquid metal as well as through the plasma surrounding the electrode. In the present time the numerical model cannot be applied for high electric current where the current is lost. In the future the numerical model will be developed to model the discharge and the ionisation of the air.

Acknowledgements

The financial support by the Austrian Federal Ministry of Economy, Family and Youth and the National Foundation for Research, Technology and Development is gratefully acknowledged.

References

[1] V. Bojarevics, E.V. Scherbinin, Azimuthal rotation in the axisymmetric meridional flow due to an electric-current source, J. Fluid Mech. 126 (1983) 413–430.
[2] V. Bojarevich, J.A. Frejbergs, E.I. Shilova, E.V. Shcherbinin, Electrically Induced Vortical Flows, Khuwer Acad. Publ, Dordrecht, Boston, London, 1989.
[3] V. Bojarevics, M. Romerio, Eur. J. Mech. B 13 (1994) 33–56.
[4] P.E. Dimotakis, R.C. Miake-Lye, D.A. Papantoniou, Structure and dynamics of round turbulent jets, Phys. Fluids 26 (1983) 3185–3192.
[5] P. Graneau, Electrodynamic seawater jet: an alternative to the propeller?, IEEE Trans Magn. 25 (1989) 3275–3277.
[6] A. Kharicha, A. Ludwig, M. Wu, Mater. Sci. Eng., A 413 (2005) 129–134.
[7] A. Kharicha, A. Ludwig, R. Tanzer, W. Schützenhöfer, Mater. Sci. Forum 649 (2010) 229–236.
[8] A. Kharicha, A. Ludwig, M. Wu, EPD Congress, San Diego, USA, 2011, pp. 771–778.
[9] A. Kharicha, M. Wu, A. Ludwig, E. Karimi-Sibaki, Influence of the earth magnetic field on electrically induced flows, J. Iron Steel Res. Int. 19 (Suppl. 1-1) (2012) 63–66.
[10] A. Kharicha, A. Ludwig, M. Wu, ISIJ Int. 54 (2014) 1621–1628.
[11] D. Liepmann, M. Gharib, The role of streamwise vorticity in the near-field entrainment of round jets, J. Fluid Mech. 245 (1992) 643–668.
[12] G.E. Mattingly, C.C. Chang, Unstable waves on an axisymmetric jet column, J. Fluid Mech. 65 (1974) 541.
[13] N.B. Morley, J. Burris, L.C. Cadwallader, M.D. Nornberg, Rev. Sci. Instrum. 79 (2008).
[14] D. Munger, A. Vincent, Magnetohydrodynamics 42 (2006) 417–425.
[15] E.E. Northrup, Some newly observed manifestations of forces in the interior of an electric conductor, Phys. Rev. 24 (1907) 474.
[16] Y. Plevachuk, V. Vasyl Sklyarchuk, S. Eckert, G. Gerbeth, R. Novakovic, J. Chem. Eng. Data 59 (2014) 757.
[17] V.Ya. Prohorenko, E.A. Ratushnyak, B.I. Stadnik, V.I. Lah, A.M. Koval, Physical properties of thermometric alloy In–Ga–Sn, High Temp. 8 (2) (1970).
[18] A.J. Reynolds, Observations of a liquid-into-liquid jet, J. Fluid Mech. 14 (1962) 552–556.
[19] A. Viilu, An experimental determination of the minimum Reynolds number for instability in a free jet, J. Appl. Mech. 29 (1962) 506.
[20] D.J. Wright, Hysteresis of the angle of contact of mercury against steel, Proc. Phys. Soc. B 68 (1955) 297.
[21] V.G. Zhilin, Yu.P. Ivochkin, I.O. Teplyakov, The problem of swirling of axisymmetric electrovortex flows, High Temp. 49 (6) (2011) 924–926.
[22] O. Zikanov, A. Thess, P.A. Davidson, D.P. Ziegler, A new approach to numerical simulation of melt flows and interface instability in Hall-Héroult cell, Met. Trans. B 31B (2000) 1541.